CHEMISTRY OF MATERIALS
Article

Chem. Mater. **2009,** *21,* 2777–2788 2777
DOI:10.1021/cm900378c

Photo and Electrochemical Characteristics Dependent on the Phase Ratio of Nanocolumnar Structured TiO_2 Films by RF Magnetron Sputtering Technique

Soon Hyung Kang, Ju-Wan Lim, Hyun Sik Kim, Jae-Yup Kim, Young-Hoon Chung, and Yung-Eun Sung*

School of Chemical & Biological Engineering & Interdisciplinary Program in Nano Science and Technology, Seoul National University, Seoul 151-742, Republic of Korea

Received February 10, 2009. Revised Manuscript Received April 20, 2009

Nanostructured titanium dioxide (TiO_2) prepared by RF magnetron sputtering was grown at substrate temperatures (T_{sub}) ranging from RT (25 °C) to 450 °C. At lower temperatures, the TiO_2 film deposited at a high sputtering pressure (12 mTorr) was amorphous. This was due to adatoms being unable to migrate effectively on the substrate. However, an increase in T_{sub} provides additional thermal energy and promotes the formation of the rutile at high temperature. The postannealing process provides additional driving force for nucleating the amorphous phase to anatase or rutile, followed by the growth of the rutile grain size. A 2.2 μm thick TiO_2 film sputtered at 350 °C had a columnar structure and showed the best performance as a photoanode layer for a dye-sensitized solar cell (DSSC), with a V_{oc} of 0.65 V, a J_{sc} of 7.93 mA/cm^2, a fill factor of 0.533, and efficiency of 2.74%. In addition, the durable electrochromic performance was also confirmed using 400 nm thick TiO_2 films sputtered at 350 °C. The improved properties were attributed to the formation of a mixed crystalline phase with anatase and rutile, a porous structure, and the narrowing of the optical band gap because of the formation of rutile, trap sites, and surface states. Furthermore, the calculated porosity of the TiO_2 film sputtered at 350 °C also showed a high value (~60%), which contributes to the increase in surface area and is in close contact to the electrolyte.

1. Introduction

TiO_2 is a typical wide band gap semiconductor that has been studied extensively in areas such as synthesis, deposition process, crystal structure, optical properties, phase stability, photosensitivity, and morphological changes.[1,2] In particular, among the three crystallographic phases, anatase, rutile (both tetragonal), and brookite (orthorhombic), anatase TiO_2 has been widely investigated on account of its photocatalytic, photoelectrochemical, and electrochromic properties.[3] However, there have been few reports on the rutile phase because of its low efficiency.[4] Despite the similar electronic structure of anatase and rutile, some significant discrepancies in electrical and optical properties have been reported.[5] Anatase, which has four TiO_2 molecules per unit cell, has lattice constants a = 3.7842 Å and c = 9.5146 Å, whereas rutile, which has two molecules per unit cell, has lattice constants a = 4.5937 Å and c = 2.9587 Å. Rutile is the most dense (density 4.25 g/cm^3) and thermodynamically stable, while anatase is metastable and less dense phase (density 3.894 g/cm^3).[6] On the other hand, the relative phase stability of anatase and rutile reverses when the particle size decreases to sufficiently low values (< 14 nm).[7] This was explained by the dominance of the higher unsatisfied charge densities of the rutile surfaces, leading to a higher surface free energy than anatase. Furthermore, it was reported that the anatase has a wider optical band gap (3.2 eV) than rutile (3.0 eV), indicating the essentially different behaviors at the fundamental absorption edge.[8] In anatase, each TiO_6 octahedron is connected to eight neighboring ones, forming a less compact structure. Therefore, excitons acting between the conduction-band electrons located on the Ti 3d states and the valence-band holes formed by the O 2p states are strongly localized due to the weak intersite transfer, which results in them being self-trapped. In rutile, each TiO_6 octahedron is connected to ten neighboring ones sharing an edge. Because of the structurally strong network, the excitons in rutile exist in the free state,

*Corresponding author. Tel: 82-2-880-1889. Fax: 82-2-888-1604. E-mail: ysung@snu.ac.kr.

(1) Bennett, J. M.; Pelletier, E.; Albrand, G.; Borgogno, J. P.; Lazarides, B.; Carniglia, C. K. *Appl. Opt.* **1989**, *28*, 3303.
(2) Wang, T. M.; Zheng, S. K.; Hao, W. C.; Wang, C. *Surf. Coat. Technol.* **2002**, *155*, 141.
(3) Yang, K.; Dai, Y.; Huang, B.; Han, S. *J. Phys. Chem. B* **2006**, *110*, 24011.
(4) Park, N. -G.; van de Lagemaat, J.; Frank, A. J. *J. Phys. Chem. B* **2000**, *104*, 8989.
(5) Weinberger, B. R.; Garber, R. B. *Appl. Phys. Lett.* **1995**, *66*, 2409.
(6) Lazzeri, M.; Vittadini, A.; Selloni, A. *Phys. Rev. B* **2001**, *63*, 155409.
(7) (a) Zhang, H.; Banfield, J. F. *J. Mater. Chem.* **1998**, *8*, 2073. (b) Dachille, F.; Simons, P. Y.; Roy, R. *Am. Mineral.* **1968**, *53*, 1929.
(8) Tan, H.; Lévy, F.; Berger, H.; Schmid, P. E. *Phys. Rev. B* **1995**, *52*, 7771.

Published on Web 05/29/2009

correlating with the structural differences. In addition, the high refractive index (3.0) of rutile has attracted considerable attention due to the efficient light scattering event, compared with that (2.7) of anatase.[9] Moreover, chemically unstable anatase TiO_2 transforms to rutile after annealing at high temperatures (>600 °C). In this situation, several methods to vary the size distribution of the nanosized TiO_2 particles and control the crystalline phases have been reported. In particular, the sol−gel process has attracted considerable attention since Grätzel's group created the highly efficient dye-sensitized solar cell (DSSC) utilizing a photoanode composed of nanoporous and interconnected TiO_2 particles.[10] This process can easily synthesize particles with various sizes and shapes, although the lengthy process and the insufficient mechanical durability have been considered the main limitation to its commercialization.[11] This paper reports the deposition of nanocrystalline TiO_2 films with a controlled anatase-to-rutile ratio by RF magnetron sputtering. In general, it is known that magnetron sputtering enables industrial processes that are applicable to large-area deposition with high uniformity at a relatively low deposition temperature, and forms high-quality TiO_2 films reproducibly.[12] On the other hand, TiO_2 films grown by magnetron sputtering cannot adsorb a large amount of dye molecules because of the lower specific surface area resulting from the compact structure compared to the TiO_2 nanoparticle based film.[13] In order to modify the inefficient TiO_2 structure, a nanoporous TiO_2 film with both anatase and rutile was prepared with increased surface area by controlling the substrate temperature (T_{sub}) during deposition. Depending on the ratio of anatase/rutile phase, a columnar TiO_2 structure composed of nanosized grains could also be produced. The TiO_2 film in the optimum anatase/rutile ratio ($\sim$1/2) also affected the long-term durability and coloration efficiency ($\sim$12%) of the electrochromic (EC) device, where there have been few reports because of its large coloration time and low coloration efficiency compared with WO_3 films.[14] This resulted from the formation of a stable structure supported by a mechanically stable rutile phase.

2. Experimental Section

2.1. Preparation of Sputtered TiO_2 Film. An optically transparent conducting glass (FTO, Pilkington TEC Glass, sheet resistance 8 Ω /sq, transmittance 77% in the visible range) was used as the substrate. The substrate was cleaned successively in ethanol and deionized (DI) water for 20 min in each step to remove any organic contamination. Titanium dioxide films with a thickness of 0.8−2.2 μm (deposition time from 2 to 5.5 h) were prepared by radio frequency (RF, 13.56 MHz) magnetron sputtering system using a 2-in. TiO_2 target (99.99%, DASOM rms) attached to a metallic Cu back plate positioned 8 cm from the substrate holder. The deposition rate of the TiO_2 film was calculated to be approximately 6.6 nm/min from a thickness of 800 nm after 2 h. Sputtering was performed in a 60 °C titled angle condition between the substrate's surface and the mean direction of the sputtered flux. The base pressure in the process chamber was $< 5 \times 10^{-7}$ Torr by diffusion pumping and the total gas pressure (P_{tot}) during deposition was 12 mTorr in an Ar (99.999%, pure) atmosphere. The substrate was rotated at a constant velocity and the applied RF power was kept at 100 W. The T_{sub} was controlled from RT (25 °C) to 450 °C using a halogen heater lamp during deposition. At the optimum condition at $T_{350\ °C}$, the deposition time was increased from the 2 to 5.5 h in order to obtain the maximum photoelectric conversion efficiency of DSSCs. Besides, for favorable applications to EC devices, a 400 nm thick TiO_2 film was prepared by 1 h deposition.

2.2. Electrode Assembly for Dye-sensitized Solar Cell and Electrochromic Device. The as-prepared TiO_2 film shows an amorphous phase, which transformed to a crystalline phase (anatase, rutile, and mixture of both phases) when thermally treated at 400 °C for 20 min under air ambient. The baked TiO_2 film was dipped into an absolute ethanol solution containing 0.5 mM *cis*-bis(isothiocyanato)bis(2,2′-bipyridy-4,4′-dicarboxylato)-ruthenium(II) bis-tetrabutylammonium (Ru 535-bisTBA, Solaronix) for 12 h in a 40° C oven. The film was then rinsed with ethanol and dried under an air stream. The used redox electrolyte consisted of 0.3 M 1-methyl-3-propylimidazolium iodide (MPII), 0.1 M LiI, 0.05 M I_2, 0.5 M *tert*-butyl pyridine (TBP) in methoxypropionitrile (MPN). Pt coated counter electrodes were prepared by spreading a drop of 5 mM H_2PtCl_6 in 2-propanol on FTO glass and heating it to 400 °C for 15 min under air ambient. Two small holes sized in 0.75 mm were made using a microdriller in both edge sides. The dye-adsorbed TiO_2 electrodes were assembled using thermal adhesive films (Surlyn, 60 μm) into the Sandwich-type cell with a counter electrode. A drop of electrolyte solution was injected into the cell. The holes were sealed using the Serlyn and a cover glass. An illuminated actual area of 0.25 cm^2 was fabricated by masking the front side.

For use in the EC device, the TiO_2 films were prepared under the same conditions and process, except for the thickness (400 nm). The EC test was carried out in a three-electrode configuration system with 2 × 2 cm sized TiO_2 film as the working electrode, a Pt wire as the counter electrode, and a saturated Ag/AgCl electrode as the reference electrode, respectively. The electrolyte of 1 M $LiClO_4$ in propylene carbonate was used after nitrogen bubbling to remove the oxygen present in the electrolyte. Pulse potential cycling was carried out up to 500 cycles in the range of −2.0 to +0.5 V for 30 s with a scan rate of 10 mV/s.

2.3. Photoelectrochemical and Electrochromic Measurements. The photocurrent−voltage ($J-V$) characteristics were evaluated using a 500 W xenon lamp (XIL model 05A50KS source units laid on AM 1.5 filter) with a light intensity of 100 mW/cm^2, which was adjusted using a NREL fabricated Si reference solar cell. The incident photon to current conversion efficiency (IPCE) were measured under a short circuit conditions using a tungsten lamp source with an illumination intensity of approximately 1 mW/cm^2 and a monochromatic light spectral bandwidth approximately 10 nm using a light source,

(9) Karunagaran, B.; Rajendra Kumar, R. T.; Viswanathan, C.; Mangalaraj, D.; Narayandass, Sa. K.; Mohan Rao, G. *Cryst. Res. Technol.* **2003**, *38*, 773.
(10) O'Regan, B.; Grätzel, M. *Nature* **1991**, *353*, 737.
(11) Takeda, S.; Suzuki, S.; Odaka, H.; Hosono, H. *Thin Solid Films* **2001**, *392*, 338.
(12) Zeman, P.; Takabayashi, S. *Thin Solid Films* **2003**, *433*, 57.
(13) Gómez, M.; Rodríguez, J.; Tingry, S.; Hagfeldt, A.; Lindquist, S. -E.; Granqvist, C. G. *Sol. Energy Mater. Sol. Cells* **1999**, *59*, 277.
(14) Ozer, N.; Lampert, Carl M. *Sol. Energy Mater. Sol. Cells* **1998**, *54*, 147.

monochromator, filters, and reflective. The EC properties were evaluated using the in situ transmittance before and after the experiment from the system attached with optics consisting of a He−Ne laser (633 nm), as the light source and a power meter for the detection of the optical signal modulation.

2.4. Characterization. The crystalline properties and the average grain sizes of the films were examined using high-power X-ray diffraction (HP-XRD, Rigaku D/MAX 2500 V diffractometer) with Cu Kα radiation operating at 40 kV and 100 mA. The surface morphology and thickness of the sputtered TiO_2 films grown at various T_{sub} were examined by field emission scanning electron microscope (FE-SEM, JSM-6330F, JEOL Inc.) operating at 10 kV. Furthermore, for a more detailed understanding of the 3D distribution in the sputtered TiO_2 film, atomic force microscopy (AFM) using a Nanoscope IIIa (Dimension 3100) with an etched silicon cantilever in tapping mode was applied to determine the crystal size, pore distribution, and surface roughness of the sputtered grown TiO_2 film. The scans were extended over $10 \times 10\ \mu m^2$ areas. The absorbance spectra were obtained using a Shimadzu model 3100 UV−vis spectrophotometer at a wavelength ranging from 350 to 900 nm at room temperature using a standard sample of bare FTO-coated glass. A PHI 670 Auger microscopy system was used to investigate the film uniformity by depth profiling, and the stoichiometric change in each element. Moreover, the chemical bonding states of each element in the TiO_2 film, depending on the T_{sub} during deposition was examined by X-ray photoemission spectroscopy (XPS) (PHI 5200 mode) using an Al K_α X-ray source in a chamber base pressure of $\sim 1 \times 10^{-10}$ Torr.

3. Results

3.1. Crystalline Properties. The structural modifications of the sputtered TiO_2 film were deduced from the variation in the deposition temperature. Figure 1 shows the XRD spectra of the TiO_2 films deposited on the FTO coated glass at various T_{sub} from 25 to 450 °C. The XRD peak related to the substrate was added to the bottom layer. The presence of the anatase (101) plane in the TiO_2 film ($< T_{150\ °C}$) was clearly identified at 25.3°. When the T_{sub} was increased above 150 °C, the (101) plane of anatase was decreased significantly, while the (110) plane of rutile appeared, which increased in intensity with increasing T_{sub}. In the temperature range 250−350 °C, a mixed phase of anatase and rutile coexisted. At $T_{450\ °C}$, the peak for the rutile (110) phase intensified, reflecting the structural modification of the sputtered TiO_2 film, dependent on T_{sub}. The phase ratio of anatase and rutile was calculated from the integrated intensity of the XRD peaks using the following formula[15]

$$W_R = \frac{A_R}{0.884A_A + A_R} \quad (1)$$

where W_R is the weight fraction of rutile, A_A is the integrated intensity of the anatase (101) plane, and A_R is the integrated intensity of the rutile (110) plane. The results showed that the anatase/rutile ratio, exhibiting a value > 1 at low T_{sub}, approaches unity at $T_{250\ °C}$, following a increase to < 1 at higher T_{sub}. The ratio of the rutile phase increased to 93.2% at $T_{450\ °C}$. The optimum ratio of the anatase/rutile phase is approximately 0.5 for favorable applications to DSSC and EC device, in which the TiO_2 film was sputtered at $T_{350\ °C}$. The average grain size (L), was calculated from the anatase (101) and rutile (110) peak at $2\theta = 25.3$ and 27.3° using Scherrer's equation,[16] respectively. Table 1 summarizes the calculated L values. In the case of the anatase (101) peak, the L values from the anatase (101) peak decreased from the 32.6 nm (25 °C) to 13.3 nm (350 °C) with increasing T_{sub}. In contrast, the L values from rutile (110) peak increased from 6 nm (250 °C) to 21.3 nm (450 °C). This may be due to the inhibition of the grain growth resulted from the formation of phase boundaries between the nanocrystalline anatase and rutile phases.[17] An annealing process was performed at 400 °C for 20 min under air ambient to enhance the crystallinity of the as-deposited films. Here,

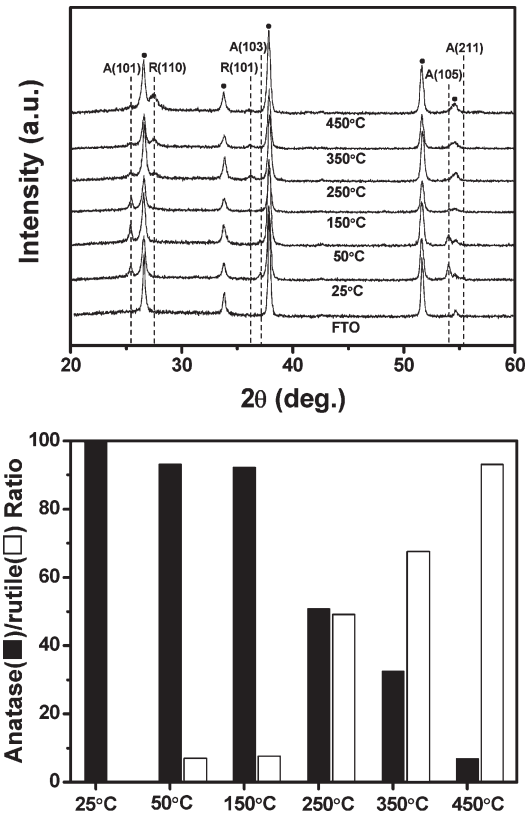

Figure 1. High-power X-ray diffraction patterns of the sputtered TiO_2 films at various T_{sub} (top side). The quantitatively calculated ratio of anatase and rutile phase at various T_{sub} (bottom side).

Table 1. Summary of the Average Crystallite Size of the TiO_2 Films Sputtered at Various T_{sub} from 25 and 450 °C, Calculated from the Scherrer's Equation

	avg. crystallite size (nm)	
T_{sub} (°C)	anatase (101) phase	rutile (110) phase
25	32.6	
50	35.9	
150	31.3	
250	20.1	6
350	13.3	20.3
450		21.3

(15) Zhang, H.; Banfield, J. F. *J. Phys. Chem. B* **2000**, *104*, 3481.

(16) Scherrer, P *Göttinger Nachr.* **1918**, *2*, 98.
(17) van der Drift, A. *Philips Res. Rep.* **1967**, *22*, 267.

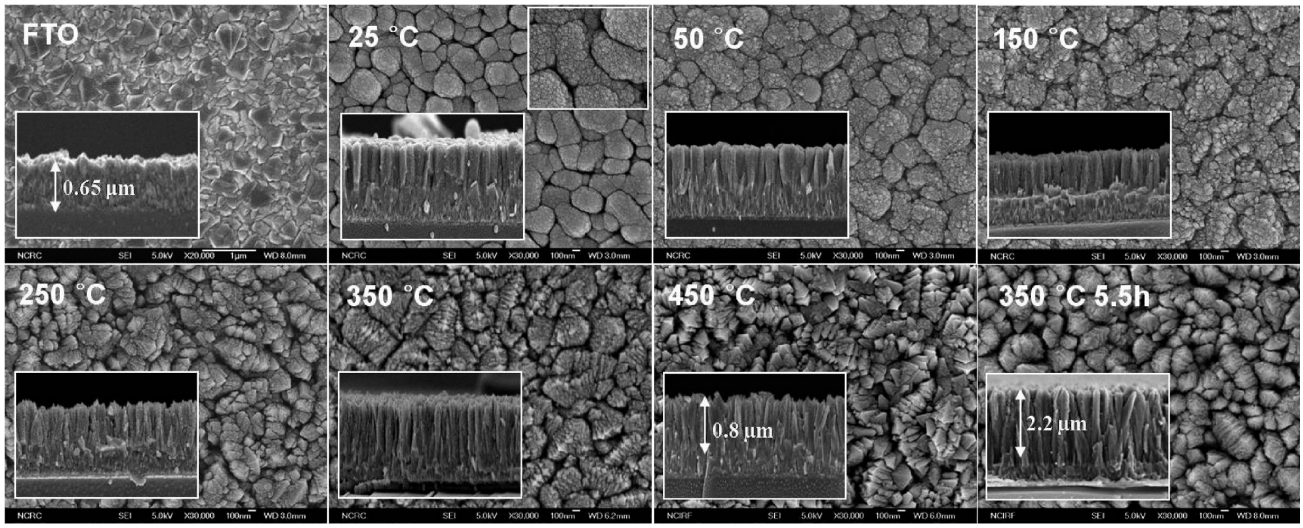

Figure 2. FE-SEM mages (surface and cross-sectional image) of the sputtered TiO_2 films at various T_{sub}. The surface and cross sectional images of the bare FTO coated substrate are shown at the left side of the top layer. In the optimum condition of $T_{350\ °C}$, the surface and side image of the TiO_2 film grown to 5.5 h are displayed at the right side of the bottom layer.

the amorphous phase transform to anatase or rutile, corresponding to the formation of an intensified rutile phase in the TiO_2 films prepared at high T_{sub} (> 200 °C), which showed an intrinsic and weak rutile phase in the as-deposited state (not shown here). Although the annealing process can contribute to the growth of grains, the presence of different phases deduced by their electrical and structural difference forms phase boundaries between each phase, blocking the growth of grains.[17] This results in a decrease in average crystallite size in the anatase or rutile phase.

Concurrently, the unit-cell volume may change in the case of a transformation to anatase or rutile is discontinuous, causing amorphization.[18] This can make a minor contribution of the remnant amorphous phase TiO_2 to the DSSCs or EC device. At $T_{450\ °C}$, the increasing T_{sub} promotes the growth of rutile, corresponding to the increased rutile grain size.

3.2. Surface Morphologies. Figure 2 shows FE-SEM images of the bare FTO coated glass and TiO_2 films grown at various T_{sub} from 25 to 450 °C. The bare FTO substrate shows a very rough surface morphology with a roughness value of approximately 100 nm. The rough substrate provides the driving force for the growth of a porous and columnar structured TiO_2 film in the situation where atoms or molecules, which have reduced kinetic energy due to collision between the target and the substrate, are preferentially deposited on the protruding parts due to the close distance in the low T_{sub}, which cannot provide sufficient thermal energy for the formation of a highly mobile cluster or islands.[19] This means that the sputtered atoms or molecules are deposited dominantly on the rugged surface. In the case of $T_{25\ °C}$, the surface morphology consisted of submicrometer-sized grains, featuring a columnar structured and microporous configuration from the cross-sectional view. In the inset of the upper side, the magnified view shows the formation of the nanosized grains protruding on the submicrometer-sized grains. The nanosized grains result in an increase in active surface area, which can contribute to the enhancement of J_{sc} in a DSSC and the total charge capacity (Q) in an EC device, and also promotes the formation of a porous TiO_2 film. With increasing T_{sub} (< 250 °C), it was shown that the projected nanosized grains grew slowly, and the micrometer-sized grains were separated into nanosized grains, maintaining a micrometer-sized morphology with a 'blooming flower-like' appearance. At $T_{sub} > 250$ °C, the surface morphology and roughness were modified by the growth of crystallites to a specific direction, possibly the (110) plane of rutile. The each column was separated by the oriented rutile crystallites, featuring a leaflike morphology from the cross-section view. This means that the specific surface area and the porosity of the film will increase. At $T_{450\ °C}$, the morphology consisted of the remarkably oriented grains, providing high surface roughness. At all T_{sub}, the deposited thickness ($\sim$800 nm $\pm$ 20 nm) of the TiO_2 film was the same. The TiO_2 film deposited for 5.5 h at $T_{350\ °C}$ shows a similar columnar structure with s thickness of 2.2 μm, which can enhance the active surface area to adsorb dye molecules, leading to an improvement in the J_{sc} in a DSSC or Q in an EC device.

Figure 3 shows AFM images of the sputtered TiO_2 films at different T_{sub}. The AFM images provide the 3D structure of the TiO_2 film in terms of depth, height, and grain size.[20] The grain size decreased abruptly with increasing T_{sub}. In particular, a TiO_2 film consisting of nanosized grains was noted in the $T_{350\ °C}$. At $T_{450\ °C}$, it was shown that the size of the composed grains was much larger than that of $T_{350\ °C}$, showing deviated result. This phenomenon was explained by the growth of rutile, which

(18) Yoganarasimhan, S. R.; Rao, C. N. R. T. *Trans. Faraday Soc* **1962**, 1579.
(19) Chen, J.-S.; Chao, S.; Kao, J.-J.; Lai, G.-R.; Wang, W.-H. *Appl. Opt*. **1997**, *36*, 4403.
(20) Namai, Y.; Matsuoka, O. *J. Phys. Chem. B* **2006**, *110*, 6451.
(21) Tanner, R. E.; Sasahara, A.; Liang, Y.; Altman, E. I.; Onishi, H. *J. Phys. Chem. B* **2002**, *106*, 8211.

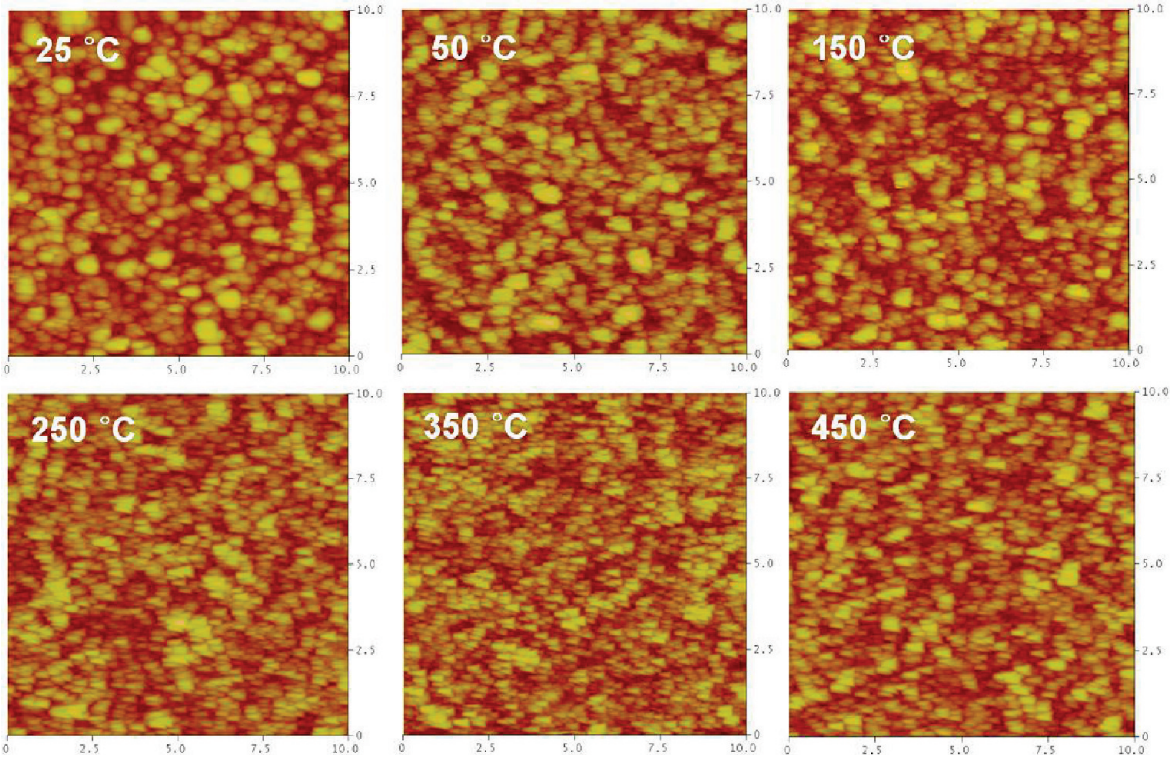

Figure 3. AFM images of the sputtered TiO_2 films at various T_{sub}.

was confirmed by XRD. In addition, the surface roughness increased linearly from 33.9 at T_{RT} to 46.05 at $T_{450\,°C}$ because of the appearance and growth of rutile. The surface roughness in the interfacial T_{sub} follows this trend.

3.3. Porosity of Three-Dimensional TiO_2 Structure. A nanoporous TiO_2 film for DSSC and EC devices is essential for the favorable permeation of the electrolyte to the entire structure. In general, the ideal porosity of the film in DSSC is approximately 50−65%, which means that pores occupy more than half of the film volume.[22] At this level, where each particle is in contact with 4 or 5 other particles, a sufficient number of interparticle connections do not cause enormous obstacles in electron motion through the trapping event from particle to particle. However, in the case of increasing film porosity (>65%), the average coordination number shifted to a low value, bringing about significant loss in the electron transport pathway because of increased winding and slow electron transport, and together the surface area for dye adsorption was also decreased. On the other hand, in the case of decreasing the film porosity (<50%), the improved interparticle connections can provide sufficient sites for the electron transport pathway, whereas a more compact film leads to a decrease in surface area, which interrupts the favorable permeation of the electrolyte and the decreased adsorption of dye molecules, thereby decreasing the cell efficiency.

Accordingly, to understand the porous structure of sputtered TiO_2 films, we require information on the film density (ρ_{film}) and refractive index (n_{film}) of each film to determine the porosity of a film. To begin with, the density of a sputtered TiO_2 film can be determined by measuring the mass, thickness, and geometric area of the film. The refractive indices of the films were evaluated using the Lorentz−Lorenz formula 2[23]

$$\frac{\rho_{film}}{\rho} = \frac{n^2 + 1}{n^2 - 1}\frac{n^2_{film} - 1}{n^2_{film} + 2} \qquad (2)$$

where ρ_{film} is the film density, ρ is bulk anatase TiO_2 density (3.9 g/cm^3), rutile TiO_2 density (4.23 g/cm^3), n is bulk anatase refractive index (2.52), rutile refractive index (2.92) at 500 nm, and n_{film} is the refractive index of the film. All the films were considered to have an anatase structure, except for the sputtered film (rutile structure) at $T_{450\,°C}$. From the refractive indices, the porosity of each sputtered film can be derived using the following eq 3[24]

$$\text{Porosity}(\%) = \left(1 - \frac{n^2_{film} - 1}{n^2 - 1}\right) \times 100 \qquad (3)$$

Table 2 summarizes the values of the film density (g/cm^3), refractive index, and porosity (%). The refractive index of the film is related to its film density. The film density decreased with increasing T_{sub}, which was followed by a decrease in the refractive index. In contrast, the film porosity increased. This may be because of the presence of small pores with a diameter <10 nm, which

(22) van de Lagemaat, J.; Benkstein, K. D.; Frank, A. J. *J. Phys. Chem. B* **2001**, *105*, 12433.
(23) Barborini, E.; Milani, P.; Cepek, C.; Sancrotti, M. *Adv. Mater.* **2005**, *17*, 1842.
(24) Mor, G. K.; Varghese, O. K.; Paulose, M.; Grimes, C. A. *Adv. Funct. Mater.* **2005**, *15*, 1291.

Table 2. Summary of the Film Density (ρ_{film}), Refractive Index, Film Porosity, Optical Band Gap (E_g), and Urbach Energy (E_u) of the TiO_2 Films Sputtered at Various T_{sub} from 25 to 450 °C

T_{sub} (°C)	ρ_{film} (g/cm^3)	refractive index	porosity (%)	E_g (eV)	E_u (eV)
25	3.30	2.13	33.9	3.06	0.319
50	2.90	1.93	49.1	3.01	0.296
150	2.81	1.89	51.9	2.76	0.390
250	2.76	1.87	53.3	2.70	0.384
350	2.53	1.77	60.1	2.62	0.456
450	3.74	2.48	31.5	2.33	0.680

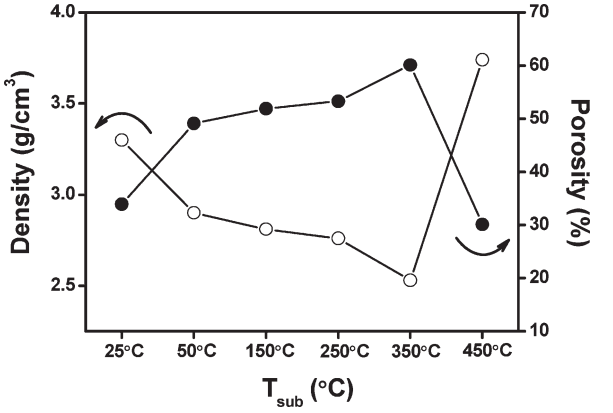

Figure 4. Comparison of the film density and porosity of the sputtered TiO_2 films as a function of T_{sub}.

substantially reduced the refractive indices of the films but do not interfere with the wavelength of the light.[25] This indicates that the small pores widely distributed in the sputtered TiO_2 film help enhance the film porosity. Therefore, a highly porous network consisting of small nanosized grains reduces the film density. The film at $T_{450\ °C}$, which was almost entirely rutile, shows a considerably different result. This may be due to the properties of rutile, which has the lowest molecular volume among the TiO_2 phases and higher refractive index than that of anatase in the bulk state. The results showed that the refractive index is dependent on the T_{sub}, and consequently on the phase content.

Figure 4 shows the relationship between the film density and porosity versus T_{sub}. The film porosity increased with decreasing film density and increasing T_{sub}. At $T_{350\ °C}$, the minimum film density and maximum film porosity were produced, leading to a high conversion efficiency of DSSC and coloration efficiency of the EC device.

3.4. Optical Properties. The absorbance of sputtered TiO_2 film was examined at wavelength ranging from 350 to 900 nm using a UV−vis spectrophotometer. Figure 5a shows the absorption coefficient (α) of the sputtered TiO_2 films grown at various T_{sub} as a function of the band gap energy (eV). Referring to the previous section, the increase in T_{sub} causes a modification of the structural and crystalline properties, finally forming a different environment in the TiO_2 lattice. This increases the absorbance of visible light, leading to a rigid shift in the absorption edge to visible wavelengths. This means that the optical band gap (E_g) decreases with increasing T_{sub}. The optical

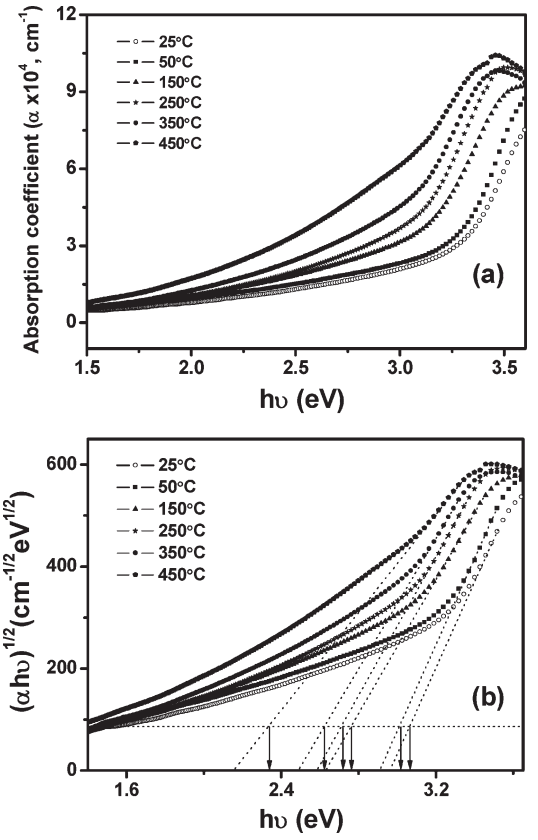

Figure 5. (a) Optical absorption coefficients α as a function of the photon energy (eV), (b) plots of $(\alpha h\nu)^{1/2}$ vs $h\nu$ for the sputtered TiO_2 films at various T_{sub}. The calculated E_g values from these plots are shown in Table 2.

E_g can be determined from the absorption coefficient α, calculated using the following formula[26]

$$\alpha(\lambda) = \frac{\ln 10^{A(l)}}{d} \tag{4}$$

where $A(\lambda)$ is the absorbance of the films and d is the film thicknesses (800 nm). In the high absorbing region ($\alpha > 1 \times 10^4\ cm^{-1}$), α obeys the following equation

$$\alpha = \frac{A}{h\nu}(h\nu - E_g)^m \tag{5}$$

where E_g is the optical band gap energy, A is a constant, and $m = 2$ in the indirect allowed transition[27,28] and $m = 1.5$ for direct forbidden transitions, which is negligible because of the weak strength. The optical band gap energy (E_g) and constant (A) estimated by plotting $(\alpha h\nu)^{1/2}$ as a function of photon energy ($h\nu$) reflects the electronic structure of the sputtered TiO_2 film. From the Table 2, it was shown that E_g decreases with increasing T_{sub}. The microporous film deposited at high temperature has a higher absorbance of visible light (450−530 nm) due to light scattering events.[29] Considering that the E_g of

(25) Yoldas, B. E. *Appl. Opt.* **1980**, *19*, 1425.
(26) Pal, M.; Tsujigami, M.; Yashikado, A.; Sakata, H. *Phys. Status Solidi (a)* **2000**, *182*, 727.
(27) Daude, N.; Gout, C.; Jouanin, C. *Phys. Rev. B* **1977**, *15*, 3229.
(28) Kang, S. H.; Sung, Y.-E. *Electrochim. Acta* **2006**, *51*, 4433.
(29) Tachibana, Y.; Hara, K.; Sayama, K.; Arakawa, H. *Chem. Mater.* **2002**, *14*, 2527.

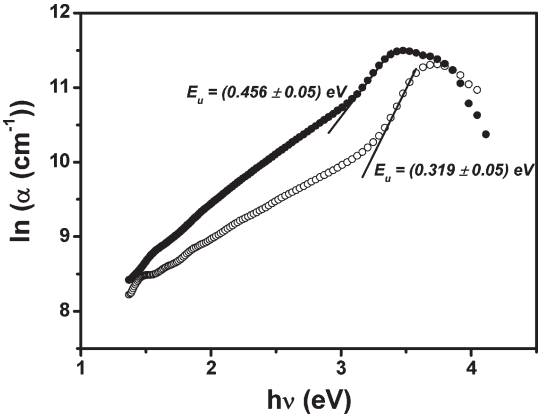

Figure 6. Plots of ln α vs $h\nu$ for the sputtered TiO_2 films at 25 °C (○) and 350 °C (●).

bulk single-crystal anatase and rutile TiO_2 is 3.2 and 3.0 eV, respectively, the considerably lower value resulted from the modification of the oxide crystal structure, a phase transformation, and morphology. In particular, because TiO_2 is generally assumed to be oxygen deficient, the defect states, e.g., oxygen vacancies, and titanium interstitials may be the main factors.[30] Furthermore, the surface state assumed from the rough and increased surface area and the grain or phase boundaries in the mixed phases might be also factors.[31] A disordered TiO_2 film containing partially amorphous phases creates localized states in the band gap, extending light absorption to visible region. Moreover, the films grown by structural modification or impurity incorporation shows an exponential absorption tail.[32]

$$\alpha = \alpha_0 \exp(h\nu/E_u) \quad (6)$$

where α_0 is a constant and the E_u is the Urbach tail. The physical meaning of the Urbach tail (E_u) is that the width of the tail of the localized states is due to the variation in size and shape distribution of the crystallinites. Figure 6 shows a logarithmic plot of the absorption coefficient as a function of the photon energy (eV). From the linear slope of the curve, the calculated values of E_u were 0.319 and 0.456 eV for the $T_{25\ °C}$ and $T_{350\ °C}$, filmsrespectively. The $T_{350\ °C}$ film shows an approximately 1 order of magnitude higher E_u value, indicating the significantly disordered state of the TiO_2 film deposited at $T_{350\ °C}$. This was estimated from the phase boundaries of the existence of mixed phases, surface states, and partially remnant amorphous layer. Table 2 shows that T_{sub} affects the increase in E_u.

3.5. Film Composition. AES measurements were performed to clarify the cause of the enhanced visible light absorption up to 700 nm and to determine the composition and uniformity of the film through depth profiling, as shown in Figure 7 a. The deposited TiO_2 film is generally

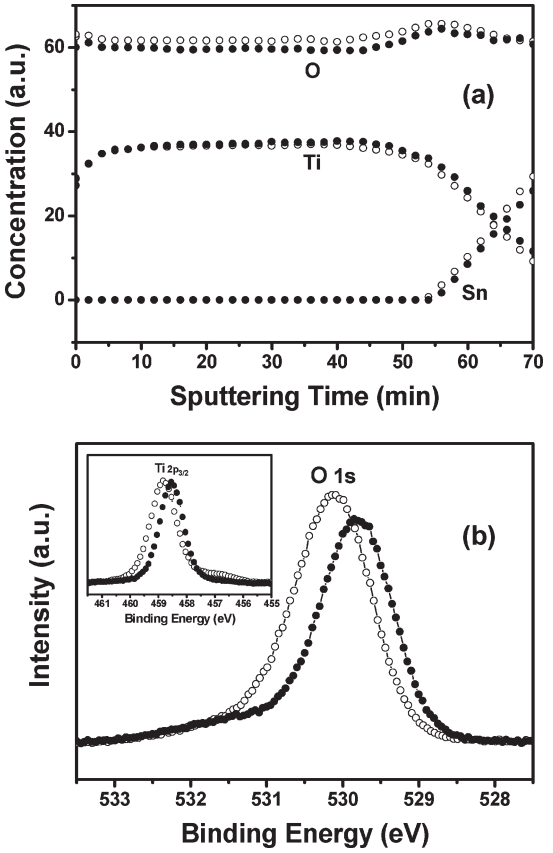

Figure 7. (a) Auger electron spectra of the TiO_2 films sputtered at 25 °C (○) and 350 °C (●) through depth profiling. (b) XPS spectra of the sputtered TiO_2 films at 25 °C (○) and 350 °C (●), describing the O 1s core level peak and Ti 2p core level peak (inset).

uniform through depth profiling, except for the interface region between the FTO substrate and TiO_2 layer where Ti is interdiffused to the FTO substrate, whereas O and Sn are out-diffused from the FTO substrate to the TiO_2 layer. The intermixing phases in the interface caused by the postannealing process may function as a resistive factor (high series resistance) for electron tunneling to the electron-collecting layer, leading to a degradation of the fill factor in DSSC.[33]

Furthermore, the $O_{25\ °C}$/Ti yield ratio of 1.91 was found to be higher than $O_{350\ °C}$/Ti yield ratio of 1.8, even though the precise stoichiometric TiO_2 (O/Ti yield ratio of 2.0) could not be determined due to the sputtering environment of pure Ar. This means Ar ion bombardment can cause an oxygen deficiency through the incorporation of Ar ions in the film.[34] Thereupon, the oxygen-deficient $T_{350\ °C}$ film shows a modified electronic structure, and together, the formation of traps sites in the intraband gap influence the optical band gap. Therefore, XPS analysis was performed to identify the state of chemical bonding of sputtered TiO_2 film, as indicated in Figure 7b. The TiO_2 film deposited at 25 °C was also used as a standard sample. Before analysis, light sputtering (5−6 Å) was performed to remove all surface contamination. The composition of both films consisted

(30) Sorrell, C. C.; Sugihara, S.; Nowotny, J. Materials for Energy Conversion Devices; Woodhead Publishing Limited: New York, 2005; Chapter 4.
(31) Kang, S. H.; Kim, J.-Y.; Sung, Y.-E. *Electrochim. Acta* **2007**, *52*, 5242.
(32) Urbach, F. *Phys. Rev.* **1953**, *92*, 1324.
(33) Cahen, D.; Ruhle, S *J. Phys. Chem. B* **2004**, *108*, 17946.
(34) Okimura, K.; Maeda, N.; Shibata, A. *Thin Solid Films* **1996**, *281*−*282*, 427.

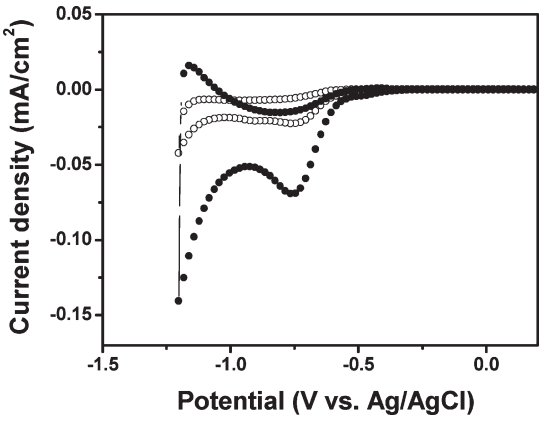

Figure 8. Cyclic voltammograms of the TiO_2 films sputtered at 25 °C (○) and 350 °C (●) in the 0.1 M NaOH solution (pH 13). The scan direction with a scan rate of 20 mV/s is positive to the negative potential. The active area is ~1 cm^2.

of Ti (459.1 eV of Ti $2p_{3/2}$), O (530.4 eV of O 1s), and C (284.3 of C 1s).[35] The binding energy scale was calibrated to the C 1s peak. The O 1s core peak of the $T_{25\ °C}$ and $T_{350\ °C}$ films was shifted to a lower binding energy side with approximately 0.26 and 0.55 eV, respectively. The amount shifted is dependent on the x value of TiO_x. Furthermore, from the area ratio, which means the quantitative amount of each element, the $O_{350\ °C}/O_{25\ °C}$ ratio derived from the integration of the O 1s peak was 0.89, highlighting the oxygen-deficient state in the film grown at $T_{350°}$.

The inset in Figure 7b shows the Ti 2p core level peaks of both films. The Ti *2*p core level peak of the TiO_2 film grown in relatively oxygen-sufficient circumstances ($T_{25\ °C}$) was shifted to a slightly lower binding energy side, with a slightly asymmetric peak with a weak shoulder on the low binding energy side (approximately 457 eV) of the main peak, which indicates the partial presence of Ti^{3+} states.[36] Besides, the Ti 2p core level of the $T_{350\ °C}$ film was also shifted to lower energy side (approximately 0.54 eV), containing a slightly weak shoulder on the 457 eV range. It is clear that the TiO_2 films grown in significantly different environments show different properties, particularly electrical, optical, crystalline, and morphological properties. The structural deviation induced from the significantly different growing environment influences the state of chemical bonding in the Ti−O lattice.

3.6. Electrochemical Analysis. Figure 8 shows the cyclic voltammograms of the both films in a 0.1 N NaOH solution (pH 13, V_{FB} of −1.14 V)[37] with a scan rate of 20 mV/s. Both voltammograms show hysteretic shape characteristics of electron charging/discharging in the nanostructured film, assuming the flow of the faradic current in the electrolyte. At $T_{350\ °C}$, the cathodic current

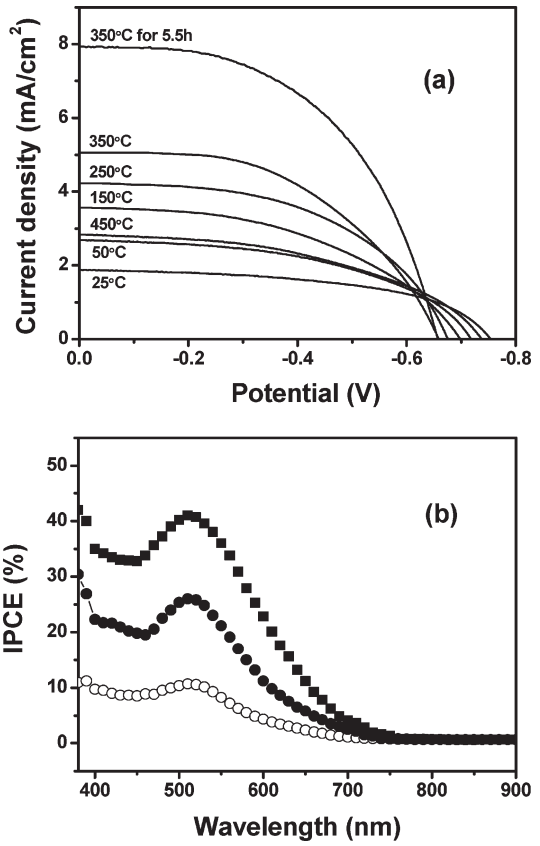

Figure 9. (a) Photocurrent density−voltage ($J-V$) characteristics of the TiO_2 films sputtered at various T_{sub} from 25 to 450 °C in a light intensity of 100 mW/cm^2 with AM 1.5 filter (illumination area: 0.25 cm^2). The $J-V$ result of the TiO_2 film deposited for 5.5 h at $T_{350\ °C}$ was also indicated. (b) IPCE spectra of the sputtered TiO_2 films at 25 °C (○), 350 °C (●), and 350 °C for 5.5 h (■) (active area: 0.36 cm^2).

mainly starts to flow at a lower potential region (−0.3 V vs Ag/AgCl) and continues over a wider potential range, compared with that of the control sample. At a potential of −0.75 V, a shoulder was observed showing an increase in current, indicating the remarkable formation of trap states in this region. It is likely that the increased surface states induced by the formation of a porous and disordered structure formed by phase boundaries and remnant amorphous phases might produce new pathways for electron transfer to the electrolyte.[38] This suggests that trap sites exist in the deep level (below −0.3 V from V_{FB}) of the band gap region, and are widely distributed. In the $T_{25\ °C}$ film, a similar curve with potential scanning was observed, with the exception of a discrepancy in the cathodic charge amount, which is qualitatively proportional to the surface area. The $T_{350\ °C}$ film shows a large cathodic charge in the range of −0.75 V and > −1 V, which shows the existence of a large surface area.[39]

3.7. Photocurrent−Voltage ($J-V$) Characteristics of DSSCs. Figure 9 shows the $J-V$ and IPCE curves of DSSCs made from the sputtered TiO_2 film grown in the various T_{sub}. From the $J-V$ curve in the Figure 9 (a) and the results summarized in Table 3, it was noticed that J_{sc} is

(35) Handbook of X-ray Photoelectron Spectroscopy; Wagner, C. D., Riggs, W. M., Davis, L. E., Muilengerg, G. E., Eds.; Physical Electronics, Perkin-Elmer: Eden Prairie, MN, 1979.
(36) Kang, S. H.; Kim, J.-Y.; Sung, Y.-E. *J. Phys. Chem. C* **2007**, *111*, 9614.
(37) (a) Rothengerger, G.; Fitzmaurice, D.; Grätzel, M. *J. Phys. Chem.* **1996**, *96*, 5983. (b) Kang, S. H.; Kim, J.-Y.; Sung, Y.-E. *Electrochim. Acta* **2007**, *52*, 5242.
(38) Kang, S. H.; Kim, J.-Y.; Sung, Y.-E. *J. Photochem. Photobiol. A* **2007**, *186*, 234.
(39) Willis, R. L.; Olson, C.; O'Regan, B.; Durrant, J. R. *J. Phys. Chem. B* **2002**, *106*, 7605.

Table 3. Summary of the $J-V$ Characteristics of the TiO_2 Films Grown at from $T_{25°C}$ to $T_{450°C}$ as a Photoanode in the DSSC[a]

	V_{oc} (V)	J_{sc} (mA/cm^2)	fill factor (%)	efficiency (%)
25 °C	0.753	1.87	53	0.75
50 °C	0.729	2.66	48.45	0.94
150 °C	0.688	3.56	48.75	1.19
250 °C	0.687	4.23	51.27	1.49
350 °C	0.659	5.06	50.59	1.68
450 °C	0.736	2.83	46.7	0.97
350 °C$_{5.5\ h}$	0.650	7.93	53.3	2.74

[a] The film deposited at 350 °C for 5.5 h is abbreviated to 350 °C$_{5.5h}$. The measurements were carried out under a one-sun condition with an illumination area of 0.25 cm^2.

increased with increasing T_{sub}, whereas the open-circuit photovoltage (V_{oc}) decreased gradually. The sputtered TiO_2 film at $T_{350\ °C}$ showed the best performance with a V_{oc} value of 0.659 V, a J_{sc} value of 5.06 mA/cm^2, a fill factor of 0.506, and an efficiency (η) of 1.68%. However, in the case of $T_{450\ °C}$, an abruptly degraded J_{sc} and fill factor, accompanied by the enhanced V_{oc}, deteriorate the efficiency. This may be due to the formation of a rutile film, which reduce the adsorption of dye molecules and decreases the rate of electron transport in the photoanode layer concomitantly with a decrease of charge collection efficiency. In this situation, the growth time at the optimum condition ($T_{350\ °C}$) was increased to 5.5 h (2.2 μm), achieving a linearly increased performance (a V_{oc} of 0.65 V, a J_{sc} of 7.93 mA/cm^2, a fill factor of 0.533, and efficiency of 2.74%), according to the thickness of the TiO_2 film. This was the best result reported thus far, suggesting that the development of an efficient dye-sensitized solar cell may be possible by optimizing the growth conditions using RF sputtering. These results were again confirmed from the measurements of the incident photon to electron conversion efficiency (IPCE).

Figure 9b shows the IPCE value as a function of the wavelength from 380 to 900 nm. The $T_{350\ °C}$ film shows higher IPEC values over the entire wavelength than the $T_{25\ °C}$ film. In particular, a remarkable increase (26%) was noted at 530 nm, indicating the amount of adsorbed dye molecules. Furthermore, the 2.2 μm thick TiO_2 film sputtered for 5.5 h at $T_{350\ °C}$ also showed the large increase in the IPCE values through the entire wavelength, leading to a high J_{sc}. In particular, at 530 nm (41%) and longer wavelengths (<700 nm), the efficient improvement in J_{sc} was illustrated by the increase in the number of adsorptive dye molecules and their light scattering effect. The light scattering events originated from the structural configuration of the TiO_2 material itself, which also contributes to the increase in J_{sc} at 450−530 nm. Overall, the light scattering phenomenon by the microporous structure and high dye loading by the increased surface area were regarded as contributing factors for the improved J_{sc}.

TiO_2 is a typical cathodic EC material, coloring when reduced at a negative potential of −2.0 V vs sat. Ag/AgCl electrode for 30 s and bleaching when oxidized at a positive potential of +0.5 V vs sat. Ag/AgCl electrode for 30 s. Referring to the bare substrate, the TiO_2 films

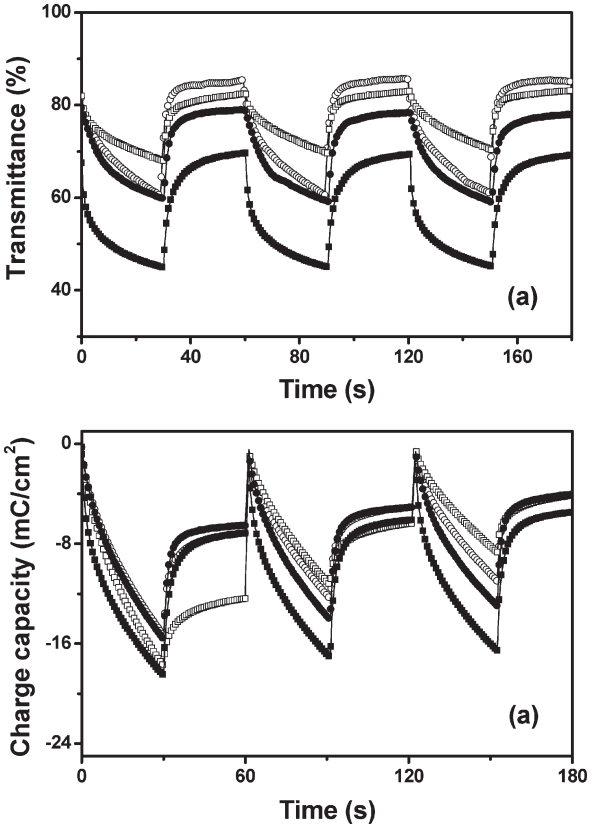

Figure 10. (a) In situ transmittance data during the continuous potential cycling. (b) Charge density data during the continuous potential cycling. $T_{25\ °C}$ (○) and $T_{350\ °C}$ (□) in the initial stage and $T_{25\ °C}$ (●) and $T_{350\ °C}$ (■) in the final stage (after 500 cycling) are depicted.

sputtered at $T_{25\ °C}$ and $T_{350\ °C}$ were continuously cycled to test the in situ transmittance. Figure 10 shows the optical transmittance (ΔT) and charge capacity (ΔQ) in the TiO_2 films sputtered at $T_{25\ °C}$ and $T_{350\ °C}$ with respect to the applied potential. In the initial stage, ΔT and ΔQ in the $T_{25\ °C}$ film were large, but decreased slowly with cycling. In the case of the $T_{350\ °C}$ film, ΔT and ΔQ were small in the initial stage, increasing gradually with cycling. It is clear that the $T_{350\ °C}$ film showed durable electrochromic properties, compared with that of the $T_{25\ °C}$ film. Therefore, in order to test the long-term stability, the sputtered TiO_2 EC cells were subjected to 500 electrochromic cycles under ambient conditions. After 500 cycles, the $T_{350\ °C}$ film shows a large ΔT during cycling, compared with that of the initial state. The rate of chronocoulometry degradation was also slow. These results are in contrast to the trend of the $T_{25\ °C}$ film.

From these results, the coloration efficiency (CE) noted by the EC performance was derived from the following equation[40]

$$CE = -\log(T_c/T_b)/\Delta Q \quad (7)$$

where T_c and T_b are the transmittances of the colored and bleached states and ΔQ is the variation of optical charge capacity. Figure 11 a shows the CE with cycling. In the

(40) Ahn, K.-S.; Nah, Y.-C.; Sung, Y.-E. *Appl. Phys. Lett.* **2003**, *82*, 3379.

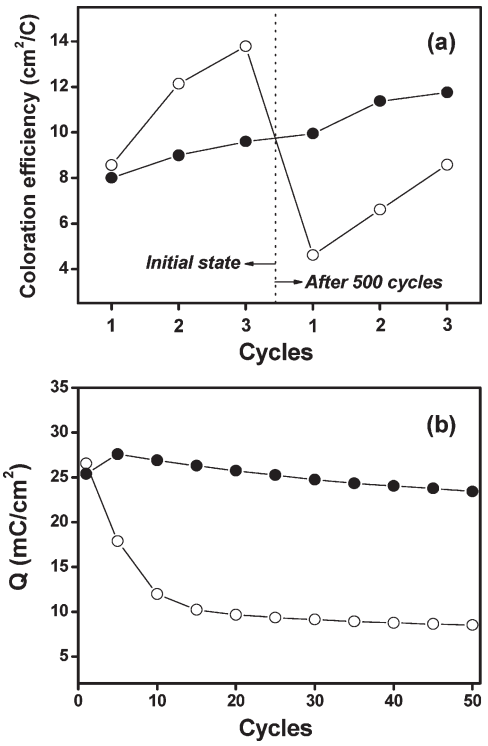

Figure 11. (a) Coloration efficiency of the sputtered TiO_2 films at 25 °C (○) and 350 °C (●) during the continuous potential cycling (initial and after 500 cycles). (b) Choronocoulometry degradation of the sputtered TiO_2 films at 25 °C (○) and 350 °C (●) during continuous potential cycling.

initial stage, the $T_{25\ °C}$ film with a pure anatase phase shows a drastically increased CE with cycling, while the increasing rate in the $T_{350\ °C}$ film progressed slowly. On the other hand, after 500 cycles, the abruptly decreased value of CE in the $T_{25\ °C}$ film corresponds to the steadily increasing CE (22%) in the $T_{350\ °C}$ film. Figure 11b shows the rapid degradation of the charge capacity of the $T_{25\ °C}$ film after 10 cycles, whereas a slowly decreasing charge capacity was observed in the $T_{350\ °C}$ film. This was attributed to the irreversible intercalated Li^+ ions from the existence of defects or trap states.[41] Overall, in the $T_{350\ °C}$ film, the long-term durability and slowly degrading charge capacity were assumed to be due to the formation of a porous and rutile mixed phase TiO_2 layer. This leads to an increase in surface area and formation of a mechanically stable film supported from the rutile phase. However, in the case of the compact and pure anatase phase in the $T_{25\ °C}$ film, the abrupt decrease in CE and Q was explained by the mechanically unstable TiO_2 layer despite the initial high charge capacity. Furthermore, the more compact structure may impede the reversible intercalation of Li^+ ions, resulting in an accumulating Li layer on the TiO_2 surface. It is possible that the deformation of the 3D structure and the filling of pores or voids occur in the $T_{25\ °C}$ film, which is processed by the continuing cycling.[42] Therefore, a mixed TiO_2 layer of anatase and rutile phases is good for an EC device in view of the long-term durability and a decreasing rate of Q, high surface area, porosity, and the formation of a mechanically supported rutile phase.

4. Discussion

The as-deposited TiO_2 films grown by RF sputtering showed a completely amorphous phase ($T_{25\ °C}$) and a partial rutile phase in the amorphous matrix ($T_{350\ °C}$). In the situation where the substrate is positioned at a distance above the mean free path of atoms or molecules and at low temperature, the thermalization of sputtered atoms occurs from their decreased kinetic energy due to an increase in collision frequency at the high sputtering pressure. The adatoms are immobilized onto the cold substrate, which prevents diffusion and migration to equilibrium lattice sites because of the insufficient thermal energy. However, at high temperatures, the less energetic particles may partially gain sufficient thermal energy, migrating to find the appropriate lattice sites. Accordingly, the preferential growth of a partial rutile phase in the amorphous matrix processed at $T_{350\ °C}$, correlating the number of nucleation sites generated initially on the substrate surface.[43] The number of nucleation sites is generally governed by the thermal energy induced by the substrate temperature and the kinetic energy of the particles impinging on the surface of the growing film.[44] Considering the growth conditions (high-pressure sputtering process and long distance between the substrate holder and target), the substrate temperature can affect film growth more significantly than the kinetic energy of the impinging particles. However, the energetic particles (TiO^+, TiO_2^+, etc.) impinging on the growing surface can influence the nucleation in a crystalline structure.[45]

These films behave differently after annealing in air at 400 °C. The crystallization of the amorphous matrix (25 °C) to anatase and the recrystallization of a partial rutile phase (350 °C) were achieved, forming an anatase/rutile mixed phase. This thermal treatment can provide the additional energy for adatoms to migrate to more stable sites, yielding a crystalline structure along with a preferred orientation in the TiO_2 film. It was reported that the (101) plane of anatase and (110) plane of rutile have the lowest surface energy, which is related to the presence of undercoordinated Ti atoms growing preferentially.[46] Therefore, the anatase (101) and rutile (110) planes are predominantly enhanced, forming mixed phases at $T_{250\ °C}-T_{350\ °C}$. This growth mechanism suggests that the appearance of a mixed phase is not due to the phase transformation from anatase to rutile but the additional driving force (thermal treatment) for nucleation from an amorphous to anatase phase and the recrystallization of a partially as-deposited rutile phase.

(41) Janke, N.; Bieberle, A. *Thin Solid Films* **2001**, *392*, 134.
(42) Dyer, C. K.; Leach, J. S. L. *J. Electrochem. Soc.* **1978**, *125*, 23.
(43) Takahashi, T.; Prabakar, K.; Nakashima, T.; Kubota, Y.; Fujishima, A. *J. Vac. Sci. Technol. A* **2006**, *24*, 1161.
(44) Shindo, W.; Ohmi, T. *J. Appl. Phys.* **1996**, *79*, 2347.
(45) Gouttebaron, R.; Cornelissen, D.; Hecq, M. *Surf. Interface Anal.* **2000**, *30*, 527.
(46) Yao, H.-C.; Chiu, M.-C.; Shieu, F.-S. *J. Electrochem. Soc.* **2006**, *153*, F237.

The lower refractive index of the $T_{350\ °C}$ film was illustrated as a thermalization effect. The sputtered particles lose their initial energetic energy of several electronvolts because of collisions with several gas atoms and become thermalized to energies of approximately 25 meV. This reduced adatom mobility at the surface leads to a porous film structure that is due to a shadowing effect, decreasing the refractive index of the film. Shadowing is a phenomenon arising from the geometric constraints imposed by the roughness of the growing film, which produces a film structure consisting of a columnar-like structure separated by voids.[47] In addition, the rough morphology of the bare FTO substrate can also contribute to the formation of a columnar-structured TiO_2 film. The upper most parts on the surface were preferentially impinged due to the close distance, growing continuously at the center. This condition forms a columnar-structured TiO_2 film, containing micrometer-sized granular-like grains with protruding nanosized grains.

The increase in surface roughness with increasing the T_{sub} can be presented by the preferential growth of a rutile phase to a specific direction, featuring a triangle-shaped surface morphology. At low temperatures, the impingement of the thermalized particles on the surface of the growing film cannot produce sites for forming nuclei, resulting in the formation of an amorphous TiO_2 film. In contrast, the TiO_2 film sputtered at $T_{350\ °C}$ may gain sufficient additional thermal energy for nucleation to rutile through substrate heating. The (110) plane is the most stable plane of rutile. Therefore, the growth of rutile by this plane increased the surface roughness, which was identified by the clear surface images. Furthermore, the nuclei sputtered at $T_{350\ °C}$ may be formed in the type of the nonwetting mode, which indicates a large contact angle (180°) with the substrate, usually forming spherical shape to minimize the surface area. Thus, the nonwetting nuclei usually orient randomly, giving rise to form a columnar structure.[48]

The change in the grain size of the anatase and rutile phases, which was dependent on T_{sub}, were explained by the lack of total energy supplied to the growing film surface. This also includes the energy of particles as impinging. A thin film with a high quality can be grown provided sufficient energy is supplied, while insufficient energy induces porous and disordered film growth, particularly in the films containing randomly mixed phases at $T_{350\ °C}$. The growth inhibition due to the randomly mixed different phases was also considered. With increasing T_{sub}, a film containing rutile was dominantly formed, concurrently decreasing in the surrounding amorphous matrix. From the FE-SEM image in Figure 2, the growth of the protruded nanograins on the surface of the micrograins occurred with increasing T_{sub}, indicating the growth of rutile in the (101) plane. It was coincident that the high content and large average crystallite sizes of rutile at $T_{sub} > 250$ °C were obtained.

The improved performance of the DSSC using the $T_{350\ °C}$ film might be due to the mixed phases of anatase and rutile and the formation of a porous structure consisting of nanosized grains. The mixed phase TiO_2 layer has attracted considerable attention for applications to DSSC rather than a pure anatase TiO_2 layer because of the high charge separation efficiency due to the high electron affinity (4.6 eV), mechanical stability to support a three-network configuration because of its high density and stability at high temperature, and light scattering effect due to its high refractive index, which enhances the absorption of visible light.[49] In this context, the TiO_2 film with mixed phases also showed the best efficiency. Moreover, the porous structure consisting of nanosized grains leads to an enhanced surface area, including increased surface roughness from the specifically directed rutile phase. This factor is closely related to the dye adsorption, which leads directly to an improvement in J_{sc}.

In brief, the factors contributing to the improved conversion efficiency are as follows: (1) The enhanced J_{sc}: the high surface area induced by forming a porous structure, the enhanced surface roughness by the predominant formation of specifically oriented rutile (110) phase, and the improved light scattering effect from the pores or voids between the micrograins and anatase/rutile coexistence phase, as confirmed by the IPCE results. (2) The degraded V_{oc}: widely distributed trap states below V_{FB}, confirmed by electrochemical analysis, including the increase in the number of surface states; oxygen vacancies resulting from the nonstoichiometric TiO_2, grain, or phase boundaries; and remnant amorphous phase. These results suggest that the significantly improved J_{sc} contributes directly to the increase in conversion efficiency, despite the slightly degraded V_{oc}. In contrast, the pure anatase TiO_2 film shows a reduction of active surface area resulting from the compact columnar structure. This factor reduces the amount of adsorbed dye molecules and blocks the favorable permeation of redox electrolyte. Furthermore, there is slight effect of light scattering in the TiO_2 material itself and dye-adsorbed state. On the other hand, the trap sites formed by the grain or phase boundaries were not considered due to the pure anatase TiO_2 layer, with a minor contribution of surface states, resulting in a high V_{oc} value. This context indicates that the surface states and grain or phase boundaries decrease the rate of electron transport and recombine with cations from the dye and redox electrolyte, inducing a decrease in V_{oc}.

Besides, it was confirmed that the bare TiO_2 film itself improves the performance for DSSC up to 5% (data not shown). In particular, the increased J_{sc} (0.298 mA/cm^2) of the $T_{350\ °C}$ film resulting from an increase in surface area and light scattering increases the conversion efficiency (0.081%). In the case of the $T_{25\ °C}$ film, a conversion

(47) Ohring, M. The Materials Science of Thin Films; Academic Press: San Diego, 1992; Chapter 5.
(48) Shirakawa, H.; Komiyama, H. *J. Nanopart. Res.* **1999**, *1*, 17.
(49) Sumita, T.; Tamaki, T.; Yamamoto, S.; Miyashita, A. *Appl. Surf. Sci.* **2002**, *200*, 21.

efficiency of 0.016% was followed by a J_{sc} value of 0.097 mA/cm^2. This shows that the effective growth of the TiO_2 film itself is essential for applications to DSSC.

Durable electrochromic properties, in the case of $T_{350\ °C}$ film, resulted from the porous structure and mechanically stable rutile phase. Although the low CE and charge capacity was revealed in the initial step, the gradually increase in CE and decrease in charge capacity were noticed. This trend is opposite to that observed with the $T_{25\ °C}$ film. Despite the minor irreversible process from the trap sites, it is possible that Li^+ ions from the electrolyte can come in intimate contact with the TiO_2 nanosized grains close to the substrate due to the porous structure and large surface area. Therefore, the CE increases with cycling. The penetration of Li^+ ions into the porous TiO_2 structure ($T_{350\ °C}$ film), rather than the compact structured TiO_2 film ($T_{25\ °C}$ film), results in the drastic decrease in charge density with cycling because the irreversible intercalation from the distribution of trap states may block the diffusion paths.[50]

The annealed TiO_2 films sputtered at 25 and 350 °C show different crystalline, optical, morphological, and chemical properties. The $T_{350\ °C}$ film with a mixture of anatase and rutile shows superior performance in the application to DSSC and EC devices. First of all, the porous structure and large surface area of the sputtered TiO_2 layer assumed by the decrease in grain size may contribute to improvement in J_{sc} in the DSSC and the increase in charge capacity and long-term stability in the EC device. Furthermore, the narrowing effect of the band gap in the nanostructured TiO_2 film results in a modification of the optical band gap, extending the light absorption to the visible region. A nonstoichiometric TiO_2 film was grown in a pure Ar ambient, regardless of the substrate temperature. The high Ti/O ratio in the TiO_2 film gives rise to increased dye adsorption supplied from the additional sites for dye adsorption, despite the decreased V_{oc}, which is caused by the formation of defect states or grain boundaries. As a result, the 2.2 μm thick columnar TiO_2 film sputtered at $T_{350\ °C}$ shows a photoelectric conversion efficiency of 2.74%, corresponding to 41% of the IPCE at 530 nm wavelength.

(50) Kavan, L.; Kratochvilová, K.; Grätzel, M. *J. Electroanal. Chem.* **1995**, *394*, 93.

5. Conclusions

The columnar structural TiO_2 films were deposited by RF magnetron sputtering for applications to dye-sensitized solar cells and electrochromic devices. The TiO_2 film grown at $T_{350\ °C}$ showed the best performance with a V_{oc} of 0.659 V, a J_{sc} of 5.06 mA/cm$_2$, a fill factor of 0.506, and a η of 1.68%, compared with that of the $T_{25\ °C}$ film (V_{oc} of 0.753 V, J_{sc} of 1.87 mA/cm^2, fill factor of 0.53, and η of 0.75%). The factors affecting the improved conversion efficiency were attributed to the increased surface area by the decrease in grain sizes induced from the anatase/rutile mixed phase, the porous structure deduced from the low refractive index, and the narrowing of the optical band gap. However, the formation of trap sites, containing defect states, e.g., oxygen vacancies and interstitial titanium and surface states, grain or phase boundaries, and the existence of the remnant amorphous phase, induced the degradation of V_{oc} in the cell. The minor decrease in V_{oc} occurred alongside the significantly enhanced J_{sc}, revealing a maximum efficiency with a V_{oc} value of 0.65 V, a J_{sc} value of 7.93 mA/cm^2, a fill factor of 0.53.3, and a η value of 2.74%. This result is the best reported thus far, giving rise to possible applications to DSSC. Furthermore, the durable electrochromic performance resulted from the porous structure and mechanically stable rutile phase in the $T_{350\ °C}$ film. These results may provide the guidelines for revise the traditional structure to a new architecture.

Acknowledgment. This work was supported in part by KOSEF (Contract R01-2004-000-10143-0) and in part by the Research Center for Energy Conversion and Storage (Contract R11-2002-102-00000-0).